

An Unexpected Transformation of Organic Solvents into 2D Fluorescent Quantum Dots during Ultrasonication-Assisted Liquid-Phase Exfoliation

Saroj Kumar Das, Ramchandra Gawas, Satadru Chakrabarty, Gunda Harini, Rishabh Patidar, and Kabeer Jasuja*

Discipline of Chemical Engineering, Indian Institute of Technology Gandhinagar, Palaj, Gandhinagar, Gujarat 382355, India

Supporting Information

ABSTRACT: Ultrasonication within organic solvents is widely used to exfoliate layered materials and produce two-dimensional (2D) nanostructures. Several 2D materials synthesized by such liquid-phase exfoliation (LPE) approaches are reported to exhibit photoluminescence. In these approaches, it is presumed that while the 2D nanostructures are derived from the layered parent material undergoing delamination, the organic solvent serves as a dispersing medium. However, in this study, we show that the organic solvent also contributes toward formation of 2D nanostructures that are optically active. We show that the bare organic solvent, when exposed to ultrasonication, transforms into 2D photoluminescent carbon quantum dots (CQDs) that display blue, cyan, green, and yellow emissions depending upon the excitation wavelength. Although this finding is intuitive, it has remained unacknowledged in the design of experiments, which require ultrasonication of layered materials in organic solvents. Our results suggest that optical properties of dispersions obtained by LPE embody a contribution not only from the 2D nanostructures derived from the layered material but also from the 2D CQDs that are formed as a natural result of the liquid medium being exposed to ultrasonication. We anticipate that this new physical insight would form an important addition to the guidelines for exfoliation and help in rightly inferring the optical properties of the 2D material dispersions produced by these methods.



1. INTRODUCTION

Ultrasonication is a versatile tool utilized in a variety of applications such as homogenization, disintegration, degassing, and surface cleaning. In recent years, the interest in ultrasonication has deepened further because of its remarkable ability to synthesize two-dimensional (2D) nanostructures.¹ For example, ultrasonication is a widely used aid to delaminate layered materials in liquids and obtain 2D materials via liquid-phase exfoliation (LPE). This technique is extensively used to prepare a variety of 2D materials, for example, graphene,² boron nitride,³ transition-metal dichalcogenides (TMDs),^{4–6} transition-metal oxides (TMOs),⁷ metal diboride nanosheets,^{8,9} and MXenes.¹⁰ Typically, in these studies, a parent layered material is added to an appropriate organic solvent and exposed to ultrasonication to yield nanosheets. It is generally assumed in such experimentations that ultrasonication only affects the layered crystals but not the organic solvent molecules. However, we show here that ultrasonication does affect the organic solvent molecules (**Scheme 1**).

In this work, we report that ultrasonication of acetonitrile alone can result in the formation of bright photoluminescent carbon quantum dots (CQDs) (**Figure 1**). These CQDs are found to contain nitrogen and exhibit bright blue fluorescence when observed under UV light. We show that the

concentration of these CQDs can be increased with an increase in the sonication duration. We further show that sonication products of other organic solvents (like butyronitrile, ethylene glycol, *N*-methyl-2-pyrrolidone (NMP), and dimethyl sulfoxide (DMSO)) also display a similar photoluminescence behavior. These findings imply that an organic solvent in itself can yield optically active nanostructures by the effect of ultrasonication. This discovery presents a new physical insight that needs to be considered in the design of experiments involving ultrasonication within organic solvents.

2. EXPERIMENTAL SECTION

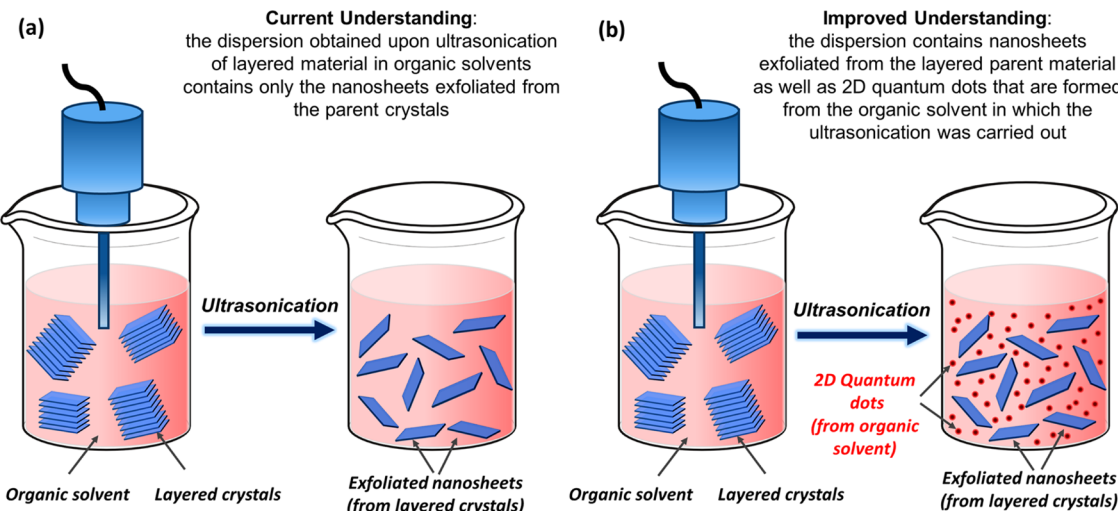
Typically, 500 mL of acetonitrile (Fisher Scientific, assay $\geq 99.9\%$) was taken in a glass beaker. It was then ultrasonicated using a flathead tip (Sonics Vibracell VC50S, 500 W, 20 kHz) for 4 h at a 60% amplitude with a pulse of 6 s on and 2 s off. Ice cooling was used to control the heat generated during ultrasonication; the bulk temperature of the solvent was maintained below ~ 30 °C throughout the ultrasonication [see **Figure S1** in the Supporting Information]. During the

Received: April 28, 2019

Revised: September 11, 2019

Published: September 13, 2019

Scheme 1. Dispersion Obtained by Ultrasonication-Assisted Exfoliation of Layered Materials in Organic Solvents Embodies a Contribution from Nanosheets and CQDs^a



^a(a) Current understanding suggests that ultrasonication affects only the layered material that delaminates into 2D nanostructures and (b) improved understanding suggests that ultrasonication also affects the organic solvent that transforms into 2D quantum dots, and thus the resultant dispersion contains both the 2D nanostructures exfoliated from the layered material as well as the quantum dots derived from the organic solvent.

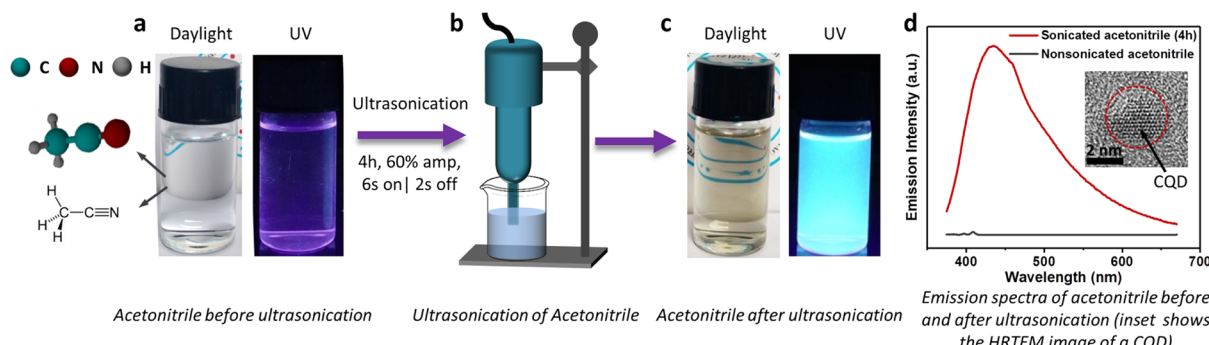


Figure 1. Formation of CQDs upon ultrasonication of acetonitrile. (a) Acetonitrile before ultrasonication is colorless in daylight and nonfluorescent under UV light. (b) Ultrasonication of the acetonitrile for 4 h results in (c) brown-yellow dispersion, which exhibits bright blue fluorescence under UV light. (d) Fluorescence emission spectra of sonicated and nonsonicated acetonitrile are shown for comparison (Ex 370 nm). The inset shows the HRTEM image of a CQD present in the dispersion.

sonication, the sample gradually turned from a colorless to brown-yellow dispersion (Figure 1) with an increase in sonication time (Figure S3). The change in color of the dispersion gave the primary indication of the formation of nanostructures in the sonicated sample. To confirm the above observation, acetonitrile from another brand (SRL, assay $\geq 99.9\%$) was also ultrasonicated, which gave a similar brown-yellow dispersion. After this, the above dispersion was passed through a $0.2 \mu\text{m}$ poly(vinylidene difluoride) (PVDF) membrane. The filtered sample was stored at 25°C until further characterization. Other organic solvents such as butyronitrile (Sigma-Aldrich, assay $\geq 99\%$), ethylene glycol (SRL, assay $\geq 99\%$), *N*-methyl-2-pyrrolidone (SRL, assay $\geq 99.5\%$), DMSO (SRL, assay $\geq 99.8\%$), and cyclohexane (SRL, assay $\geq 99\%$) were also ultrasonicated using the same method as that for acetonitrile (note: we usually run the probe sonicator for 40 min in a single cycle and maintain an interval of 2–3 h between each cycle of ultrasonication).

3. RESULTS AND DISCUSSION

The observations shown in the current study were made inadvertently while pursuing the exfoliation of a parent layered material in an organic solvent. Our original aim was to exfoliate layered metal diborides by ultrasonication in acetonitrile. As a control to the above experiment, we had to conduct the ultrasonication of acetonitrile alone. When we ultrasonicated the colorless acetonitrile for 4 h with an ultrasonication power of 500 W and a frequency of 20 kHz, a brown-yellow dispersion appeared (Figure 1a,b). The bulk temperature of the experiment was maintained below 30°C to minimize the temperature effect, which originates from the solvent and controls the reaction environment (Figure S1). To our surprise, this dispersion exhibited bright blue fluorescence under UV light (Figure 1c,d).

The emergence of fluorescence by mere ultrasonication of acetonitrile has not been reported before. Therefore, to verify this unexpected result, we revisited our experiments. We first considered the possibility that the fluorescence could be due to impurities present in acetonitrile. This possibility was discounted by the observation that nonsonicated acetonitrile

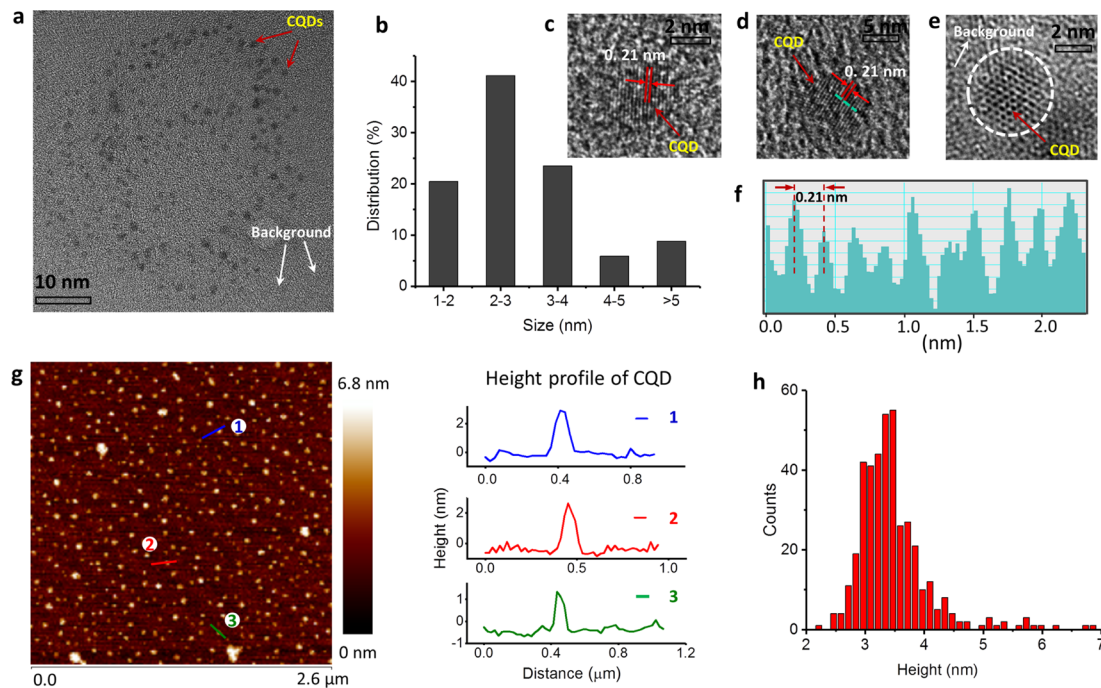


Figure 2. Structural and morphological evidence of the QDs formed after ultrasonication. (a) TEM image of the QDs on a Cu grid coated with an ultrathin amorphous carbon film. (b) Lateral size distribution of the QDs obtained from TEM analysis. (c–e) HRTEM images of the QDs showing their size to be <10 nm; corresponding line profile analyses shown in (f) reveal a lattice spacing of ~ 0.21 nm. (g) AFM image of the QDs and corresponding height profile suggest its thickness to be ~ 3 nm. (h) Height distribution histogram obtained from AFM images implies that the majority of CQDs have a thickness of <4 nm.

from the same batch did not exhibit any fluorescence (Figure 1a). We then speculated that the fluorescence could arise from foreign particulates inadvertently acquired from the experimental setup. To assess this, we designed a control experiment by immersing the ultrasonic probe in acetonitrile for a similar duration of 4 h but without switching on the sonicator. The control sample remained colorless and did not show any fluorescence under UV light (Figure S2). This led us to conclude that the observed fluorescence is not due to any processing contamination; rather, it solely results from the ultrasonication process. This is further supported by the observation that the dispersion became increasingly brown-yellow upon increasing the sonication duration from 0 to 240 min, suggesting an increased concentration of the dispersed phase (Figure S3).

We then looked into other possible sources from which the fluorescent dispersed phase could have formed. Either it might have originated *in situ* by a sonochemical transformation of acetonitrile or it could have formed as a result of metal particulates shearing off the titanium alloy present in the ultrasonic probe. To determine the source of fluorescence, the dispersed phase was recovered by evaporating the solvent to obtain a dark brown residue. X-ray photoelectron spectroscopy (XPS) of this dark brown residue did not exhibit any signals corresponding to Ti (Figure S4), thus excluding the possibility of it originating from the ultrasonic probe. This observation implies that the fluorescent dispersion is formed from acetonitrile.

To characterize the ultrasonicated acetonitrile in detail, the as-obtained brown-yellow dispersion was analyzed under a transmission electron microscope (TEM) by depositing on a carbon-coated Cu grid. The TEM images shown in Figure 2a provide the primary evidence for the formation of nanostruc-

tures, which are well-dispersed and spherical in morphology. We measured the lateral size of ~ 50 such nanostructures, and their size distribution is presented as a histogram in Figure 2b. Their mean size is found to be in the range of ~ 2 to 3 nm. Thus, we refer to these nanostructures as quantum dots (QDs). High-resolution TEM (HRTEM) images of these QDs are shown in Figure 2c–e. These QDs are found to be crystalline as revealed by the presence of distinct lattice fringes (Figure 2c,d). The line profile analyses of these diffraction fringes show an in-plane lattice spacing of ~ 0.21 nm (Figure 2f), which corresponds to the (100) plane of graphitic carbon.^{11–14} In Figure 2e, the QDs clearly show a hexagonal honeycomb arrangement of atoms similar to that of graphite (marked inside a circle). More such TEM and HRTEM images confirming the formation of QDs and their graphitization are provided in Figure S5. The ultrasmall dimension of the nanostructures is also evident in the atomic force microscope (AFM) images shown in Figure 2g. They are found to be scattered on the AFM substrate, mostly without any noticeable agglomeration. We utilized the AFM images to determine the apparent thickness of these nanostructures. For example, the inset of Figure 2g shows the height profiles of selected QDs marked 1, 2, and 3. Height profiles of several such QDs are used to generate the histogram presented in Figure 2h. From this, the mean thickness of the QDs is estimated to be in the range of ~ 3 to 4 nm.

To investigate the chemical composition of the QDs, the dispersion was deposited onto a Si/SiO₂ substrate and analyzed by XPS. The survey scan in Figure S4 indicates the presence of carbon (C) and nitrogen (N) in these nanostructures. The relative content of N and C is calculated to be 4.2 and 95.8%, respectively, suggesting that these nanostructures are nitrogen-containing carbon quantum dots

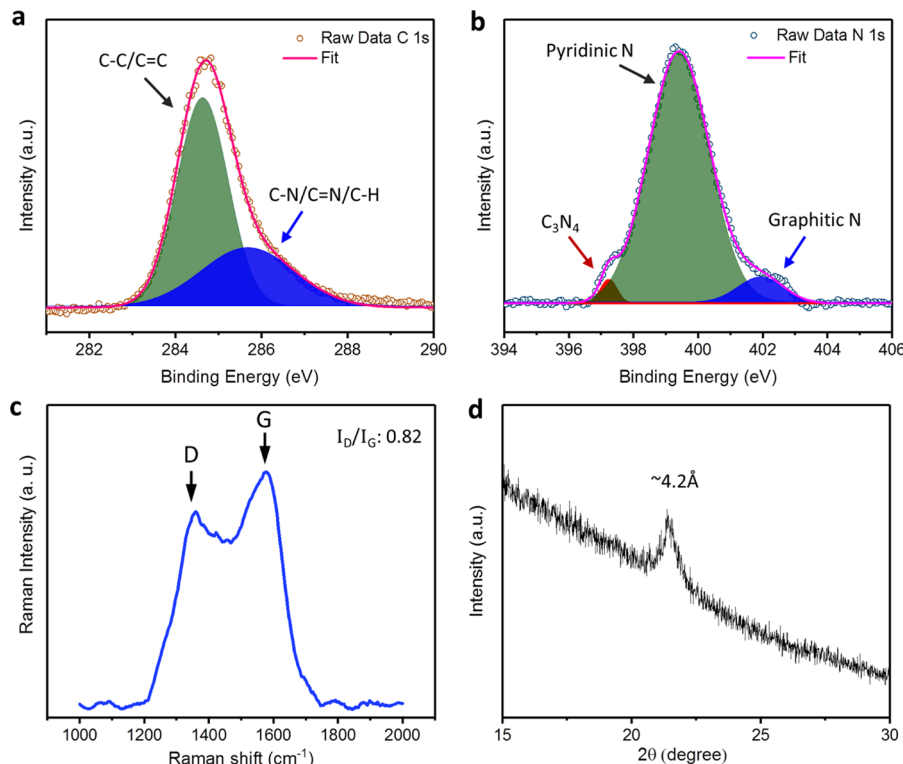


Figure 3. Spectroscopic characterization of CQDs. High-resolution XPS spectra of (a) C 1s and (b) N 1s of the synthesized QDs showing its elemental constituent as C and N. Their deconvoluted peaks suggest that most of the carbons are in the graphitic form. The formation of CQDs is further confirmed by their Raman spectrum, which displays the G (1359 cm^{-1}) and D (1577 cm^{-1}) bands characteristic to the graphitic planes. (d) XRD pattern of CQDs showing a peak at 21° corresponds to a *d* spacing of $\sim 4.2\text{ \AA}$.

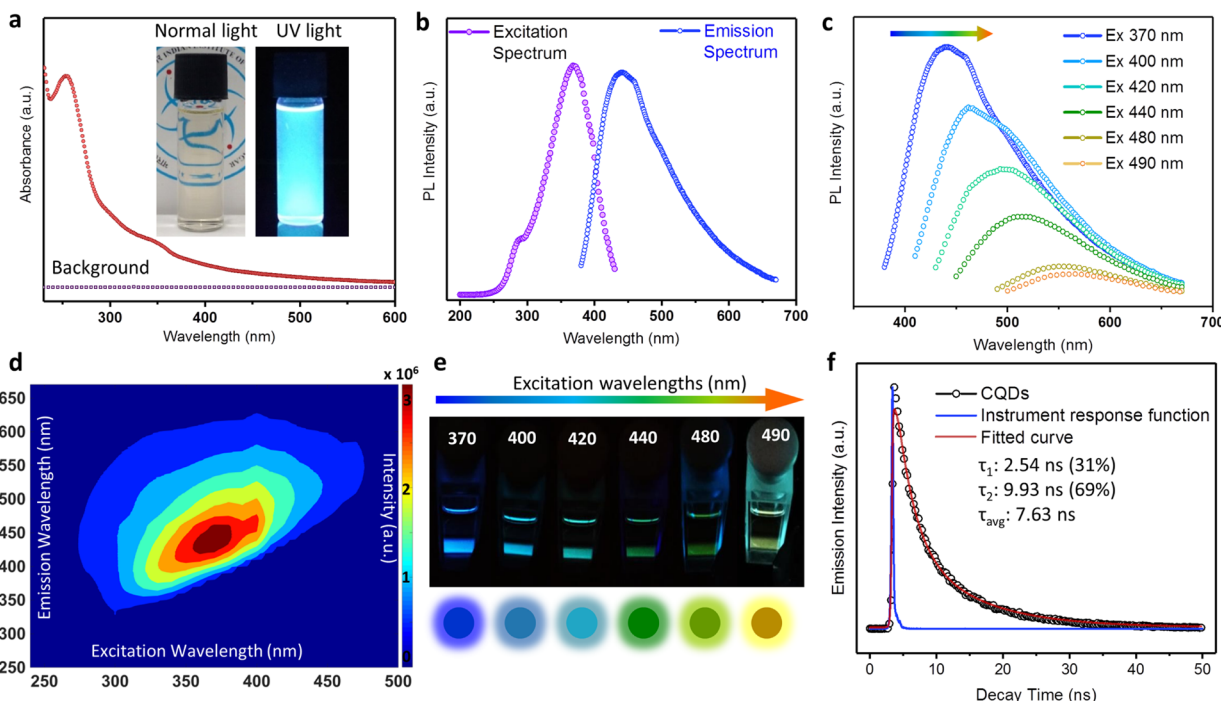


Figure 4. Optical properties of CQDs. (a) UV-visible absorption spectrum of CQD dispersion along with nonsonicated acetonitrile as a solvent background (inset: photograph of CQD dispersion in daylight and its fluorescence image under excitation of 365 nm UV light). (b) Photoluminescence excitation and emission spectra of CQDs. (c) Photoluminescence emission spectra recorded with excitation of 370 to 490 nm and (d) their corresponding fluorescence excitation–emission map. (e) Photograph of the CQD dispersion excited at various excitation wavelengths. (f) Time-resolved fluorescence decay profile measured with excitation at 370 nm and emission at 440 nm. The inset shows the lifetime data and the parameters generated by the exponential fitting.

(CQDs) (see the calculation section in the Supporting Information and Table S1). To understand the nature of chemical bonds present in nitrogen-containing CQDs, we analyzed the high-resolution XPS spectra of C 1s and N 1s (Figure 3). The fitting of the C 1s spectrum (Figure 3a) shows the presence of two daughter peaks, which are ascribed to graphitic or aliphatic carbon ($C-C/C=C$, 284.6 eV) and nitrous carbon ($C-N/C=N$, 286.0 eV).^{11,15–18} Likewise, the deconvoluted N 1s spectrum shown in Figure 3b indicates three peaks at 397.2, 399.4, and 401.9 eV, which are attributed to the N in a beta- C_3N_4 structure, N in a pyridinic-like structure, and graphitic-like nitrogen/N–H groups, respectively.^{14,15,18,19} Their relative contents are 6.8, 91.0, and 2.2%, respectively, calculated by the integrated area obtained from XPS (see the calculation section in the Supporting Information and Table S2). This suggests that the dominant nitrogen is mostly in a pyridinic form. We note that deliberate incorporation of a heteroatom in CQDs, especially N, has been a prime focus in many literature reports owing to the superior performance of the doped CQDs over pure CQDs. Most of these methods involve harsh and complex synthetic processes.²⁰ In contrast, this work has the advantage that nitrogen was inherently incorporated in the CQDs by simply choosing a nitrogen-containing source during ultrasonication. To study the functional group present on the CQDs, FTIR spectroscopic analysis was carried out. As shown in Figure S17, the absorption bands in the range of 3200–3300 cm^{-1} and 2850–2960 cm^{-1} are ascribed to the N–H and C–H bond stretching vibrations, respectively.^{21,22} Similarly, the bands at around 1650 and 1450 cm^{-1} are attributed to the typical stretching of the C=N and C–N bonds.²¹ In addition, the bands observed at 1075, 879, and 740 cm^{-1} are assigned to the out-of-plane and in-plane deformation of aromatic C–H.¹⁴

Generally, CQDs exhibit a characteristic Raman spectrum (D and G bands) due to the vibration of carbon atoms. To check this, we subjected the CQDs to a 532 nm laser and observed the resultant Raman spectra wherein two dominant peaks at 1359 and 1577 cm^{-1} were revealed (Figure 3c). The first peak at 1359 cm^{-1} is assigned to the characteristic D band associated with the vibrations of sp^3 -hybridized carbon. Meanwhile, the second peak at 1577 cm^{-1} is attributed to the G band produced by the vibrations of sp^2 -bonded carbon atoms.^{12,14,23–26} The sp^3 -hybridized carbon in the sample is expected to originate from the incorporated nitrogen in the CQDs. The relative intensity of the disordered D band to an ordered G band (I_D/I_G) is calculated to be 0.82.^{11,25,26} The X-ray diffraction (XRD) pattern of CQDs shows a reflection centered at 21°, which corresponds to the (002) plane of the graphitic structure (Figure 3d).^{24,27,28} This is in agreement with the XRD data reported for other nitrogen-containing CQDs.^{18,24,27–29}

Because CQDs are known to exhibit quantum confinement, it is likely that they may show peculiar optical properties. To test this, we performed UV-vis and PL (photoluminescence) spectroscopy of the CQD dispersion. To obtain the true optical absorption spectrum of the CQD dispersion, we subtracted the absorption data of the nonsonicated solvent (as background). Shown in Figure 4a is the UV-vis absorption spectrum, which exhibits two peaks centered at ~254 and ~350 nm with an absorption edge at ~500 nm. Generally, the peak below 300 nm is attributed to the $\pi \rightarrow \pi^*$ transition of aromatic domains ($C=C$ of sp^2 C domain in sp^3 C matrix).³⁰ The shoulder at ~330 to 365 nm in the absorption spectrum is

assigned to the $n \rightarrow \pi^*$ transition of nitrogen-containing groups and sp^2 domains.¹⁴ Given that the CQD dispersion absorbs light in the UV region, we hypothesized that they might emit light in the visible region. In anticipation of this, we observed the dispersion under a UV transilluminator (Ex 365 nm) and found it to emit bright blue fluorescence (inset of Figure 4a). Intrigued by the naked eye observation of blue fluorescence, we attempted to verify it by PL spectroscopy (Figure 4b). The emission spectrum indeed exhibits a strong peak at ~440 nm corresponding to the blue fluorescence. The excitation spectrum reveals two peaks at ~290 and ~370 nm, which are correlated with the two transitions at 4.27 eV (290 nm) and 3.35 eV (370 nm), respectively. These electronic transitions can be considered as transitions from the highest occupied molecular orbitals (HOMOs) to the lowest unoccupied molecular orbitals (LUMOs), as demonstrated in Figure S6. The energy difference between the σ and π orbitals is determined to be 0.92 eV (ΔE). This value is well below the required value ($\Delta E < 1.5$ eV) for the existence of a triple ground state, implying that this is a reasonable mapping (see description in Figure S6 for a more detailed explanation).³¹ The observed fluorescence is possibly produced by the irradiation decay of activated electrons from the LUMO to the HOMO.^{29–31} These CQDs also exhibit an excitation-dependent PL behavior. It means that a change in excitation wavelength results in shifting of the emission peak to a newer position, thereby leading to a different emission color. Here, we explored such a behavior by exciting the CQDs at wavelengths ranging from 370 to 500 nm and collecting their corresponding emission spectrum (Figure 4c). The emissions are found to be red-shifted from 400 to 550 nm, and their intensity is observed to decrease with an increase in the excitation wavelength. This is also evident in the 2D excitation emission contour map of the CQDs shown in Figure 4d. The corresponding digital photographs captured at those excitation wavelengths produce multiple emissions ranging from blue to yellow (Figure 4e). It can be noted that the most intense emission is blue (Ex 370 nm, Em 440 nm), which gradually decreases to the least intense yellow (Ex 490 nm, Em 565 nm). This observation agrees well with the PL data presented in Figure 4c. This excitation-dependent behavior is likely due to the presence of nitrogen in the CQDs.^{14,32} The emission spectrum for the nonsonicated acetonitrile was also recorded as reliable control, which did not show any peak confirming its nonfluorescent nature (Figure 1 and Figure S3). It is worthwhile to mention that the acetonitrile samples that were ultrasonicated for durations less than 240 min also exhibited similar emission behaviors, albeit with less intensities. We observed that acetonitrile samples sonicated for different durations (ranging from 20 to 240 min) exhibited the same emission maximum wavelength. An increase in the duration of ultrasonication only led to an increase in the intensity of the emission, suggesting a larger number of CQDs are being formed upon increased exposure to ultrasonication (Figure S3). These results suggest that CQDs form even when the ultrasonication durations are as low as 20 min, albeit their concentration is less when compared with organic solvent samples ultrasonicated for longer durations.

The fluorescence decay profile of the CQDs is shown in Figure 4f (see the calculation section in the Supporting Information). The obtained data is fitted to a double exponential decay function, and the parameters generated after comparing with respect to the instrument response

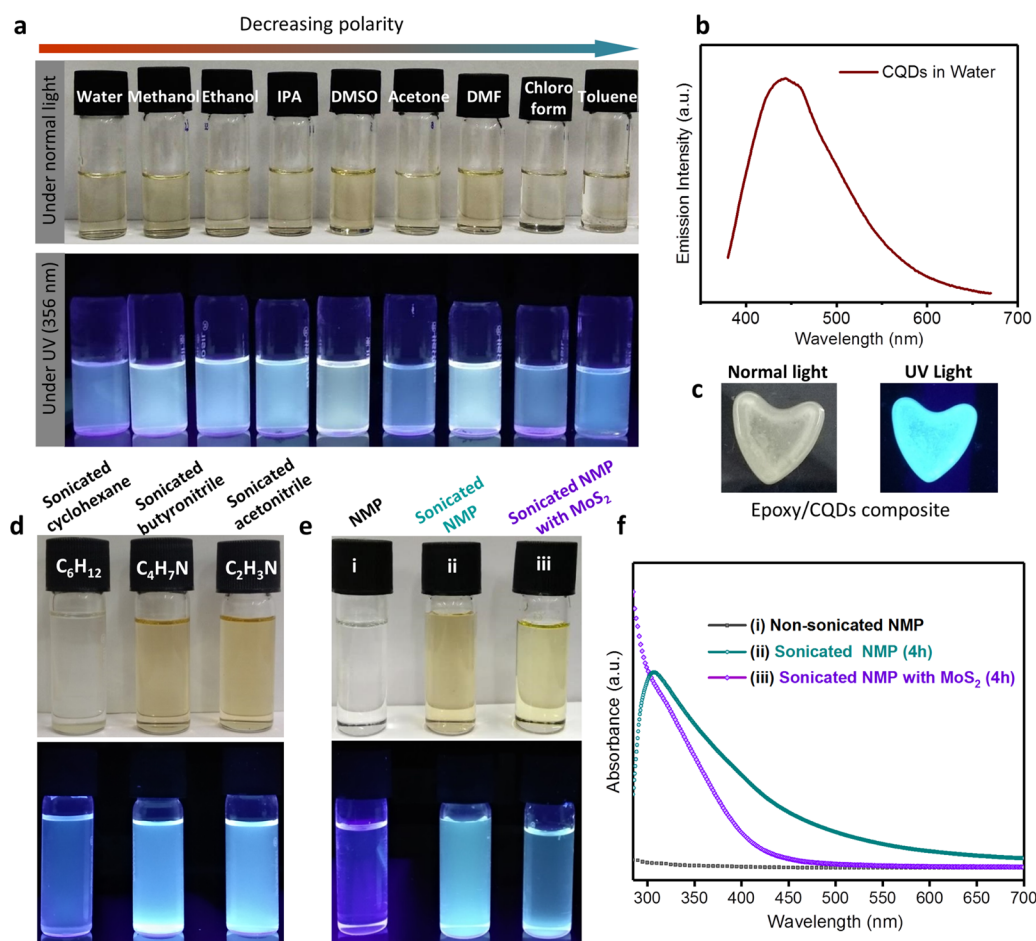


Figure 5. Dispersion behavior and mechanism of CQD formation. (a) CQDs are redispersed in different solvents in normal light (top) and under UV light (bottom). (b) PL spectrum of water-soluble CQDs at 370 nm excitation is found to be identical with that of the sonicated acetonitrile. (c) CQD-based epoxy composite under normal light (left) and under UV light (right). (d) Ultrasonicated cyclohexane (C_6H_{12}), butyronitrile (C_4H_7N), and acetonitrile (C_2H_3N) in normal light (top) and under UV (bottom). (e) Nonsonicated NMP (i), sonicated NMP (ii), and 2D MoS₂ nanostructures prepared by sonication in NMP (iii) under normal light (top) and under UV light (bottom). Their corresponding UV-visible absorption spectra are shown in (f).

function (IRF) are listed as an inset of Figure 4f. From this, the average lifetime value is calculated to be 7.6 ns. The nanosecond lifetime of CQDs suggests that they can be well-suited for optoelectronic applications. We then calculated the relative quantum yield of these blue fluorescent CQDs to be ~15% using anthracene as a reference (see the calculation section in the Supporting Information and Table S3). This value is reasonably high considering that no external surface passivation is carried out during the synthesis.²² The quantum yield can be further improved if their surface is passivated using poly(ethylene glycol) or metals typically reported for other CQDs.³³ These QDs are found to be stable for at least 6 months without any apparent precipitation at room temperature (Figure S7). The concentration of the CQDs was calculated to be 0.06 mg/mL (see the calculation section in the Supporting Information for details).

For any biological and optoelectronic applications, the CQDs should be soluble in aqueous as well as different organic solvents. Hence, to test their solubility, we evaporated the residual acetonitrile from the CQD dispersion to obtain a dark brown residue of the CQDs (Figure S7). To this residue, different polar and nonpolar solvents were added and mixed thoroughly. Shown in Figure 5a (top) are the samples obtained after redispersing CQDs in a range of solvents arranged in

order of their decreasing polarity value, namely, water, methanol, ethanol, IPA, DMSO, acetone, DMF, chloroform, and toluene. The CQDs were found to redisperse well in most of the solvents to form a distinct brown-yellow dispersion. Under UV light, these dispersions emitted strong blue fluorescence (Figure 5a bottom). Interestingly, the blue emissions can be seen even after irradiation with both UV and normal light together (Figure S8). The water solubility of CQDs is also evident in their emission spectra (Figure 5b), which is very similar to the sonicated acetonitrile (Figure 4b). These observations suggest that CQDs are highly soluble in various polar as well as nonpolar solvents. Thus, it can be ascertained that the CQDs are amphiphilic and can be employed in several practical applications. In addition, we show that CQDs can be uniformly incorporated in an epoxy polymer matrix to form a fluorescent composite (Figure 5c).

The bright fluorescence exhibited by these CQDs could be attributed to the existence of heteroatoms (e.g., nitrogen) in the CQD. Generally, heteroatoms such as nitrogen, oxygen, or sulfur can incorporate into the CQD lattice during the synthesis and disrupt the regular sp^2 hybridization of C atoms. Because of this disruption, defect sites are created in CQDs. The radiative combination of the excitons trapped by these defect sites is considered to be the possible luminescence

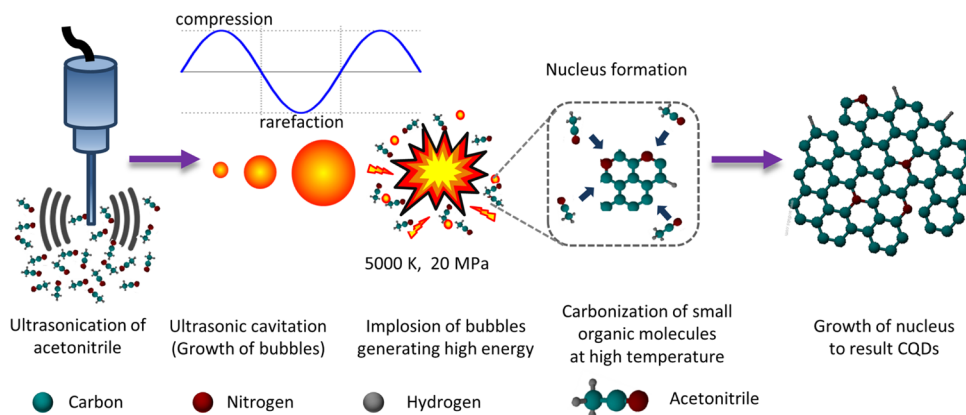


Figure 6. Illustration of the possible mechanism underlying the formation of CQDs during ultrasonication of organic solvents.

centers in the CQDs, which result in fluorescence as reported earlier.^{20,21,23} Herein, as evidenced by the XPS results, the CQDs exhibit the presence of N heteroatoms (Figure 3b). The Raman analysis in Figure 3c further suggests that this introduced nitrogen indeed disrupts the regular sp^2 hybridization of C atoms.^{22,23} In order to validate this further, we posit that a solvent, which is similar to acetonitrile, should also transform into a fluorescent dispersed phase upon ultrasonication. To test this, we chose butyronitrile (C_4H_7N) as the starting solvent and ultrasonicated it with the same procedure as followed for acetonitrile. We observe that the resultant sample also turns from a colorless to brown-yellow dispersion and emits bright blue fluorescence under UV light (Figure 5d middle) similar to ultrasonicated acetonitrile (Figure 5d right). This appearance of fluorescence is indicative of the formation of CQDs in the sonicated butyronitrile (Figure S9). To further confirm the role of heteroatoms, we selected other starting solvents such as ethylene glycol ($C_2H_6O_2$), DMSO (C_2H_6SO), and NMP (C_5H_9NO) oxygen, sulfur, and nitrogen heteroatoms. The samples obtained after 4 h of ultrasonication of these solvents are shown in Figure S10 (ethylene glycol) and Figure S13 (DMSO and NMP). The results are remarkable as it is clearly seen that these samples also emit bright blue luminescence in agreement with the observations for ultrasonicated acetonitrile and butyronitrile. Subsequently, we chose another starting solvent, namely, cyclohexane, which does not contain any heteroatoms. We observe that the ultrasonicated cyclohexane shows a different behavior. The blue emission from this sample is very weak (Figure 5d, left) in comparison with ultrasonicated butyronitrile. This behavior agrees reasonably well while comparing their fluorescence intensities at 370 nm excitation (Figure S11). From this analysis, it is clear that the emission intensity for sonicated butyronitrile or ethylene glycol (which contains heteroatoms) is higher than that for sonicated cyclohexane (which does not contain any heteroatom). It indicates that the existence of heteroatoms such as nitrogen or oxygen in the starting solvent leads to brighter fluorescence in their corresponding sonicated samples. The additional characterization data for sonicated butyronitrile (Figure S9), ethylene glycol (Figure S10), and cyclohexane (Figure S12) can be found in the Supporting Information.

Our results suggest that organic solvents such as acetonitrile, butyronitrile, cyclohexane, ethylene glycol, NMP, and DMSO can transform into optically active CQDs under the effect of ultrasonication. Although this finding is intuitive,^{34–36} it has

remained unacknowledged in the design of experiments, which require ultrasonication of layered materials in organic solvents. This finding has an important implication for liquid-phase exfoliation because these solvents are conventionally used in the ultrasonication-mediated synthesis of 2D nanostructures (e.g., titanium disulfide,³⁷ black phosphorus,^{38,39} molybdenum disulfide,⁴⁰ tungsten disulfide,⁴¹ and carbon⁴²). To demonstrate the relevance of our results, we exfoliated MoS₂ in NMP following a protocol that is known to yield 2D MoS₂ nanostructures (referred to as s-MoS₂-NMP).^{40,43} As a control to the above experiment, we also ultrasonicated NMP alone without any addition of MoS₂ (referred to as s-NMP). We observe that both s-NMP and s-MoS₂-NMP exhibit a similar brown-yellow color as well as similar blue luminescence under UV light (Figure 5e). The similarity is also evidenced by comparison of their UV-visible spectra (Figure 5f). We observed that while s-MoS₂-NMP absorbs in the range of 300–400 nm (as reported in the literature^{40,43}), s-NMP also displays a strong absorption in the same region. This validates the fact that the formation of optically active nanostructures from the organic solvents should be acknowledged while interpreting the optical results of the exfoliated 2D materials.

The possible mechanism of formation of fluorescent CQDs can be explained as follows. The ability of ultrasonication to transform the organic solvent molecules into quantum dots can be attributed to the phenomenon of cavitation associated with it. Typically, CQDs are synthesized via a solvothermal route wherein the carbon core is formed as a result of condensation, polymerization, and carbonization of organic molecules under high temperature and pressure conditions.^{12,20,44–48} It has been established that ultrasonication can facilitate similar conditions at localized spots. In the present study, we posit that similar conditions are facilitated by ultrasonication (Figure 6). The ultrasonication process generates alternating low-pressure (rarefaction) and high-pressure (compression) waves in the solvent. Because of this pressure difference, transient vacuum microbubbles (cavities) start forming in the reaction medium. Subsequently, these microbubbles grow through rectified diffusion and coalescence to reach a critical size. After reaching the maximum size, these bubbles collapse violently to develop local temperatures up to 2000–5000 K, pressures up to 20 MPa, and heating/cooling rates up to 10^9 K s^{-1} .^{1,49,50} We posit that acetonitrile molecules in the vicinity of busted microbubbles undergo carbonization to produce an intermediate carbon nucleus. The carbonization process may have been a result of one or many of the following chemical

reactions, such as hydrolysis, decarboxylation, dehydration, aromatization, and polymerization.^{44,51,52} Finally, the nucleus grows in the sample to form a stable aromatic carbonaceous structure.^{51,53,54} During this process, some of the nitrogen molecules in the acetonitrile become incorporated into the carbon skeleton, thereby resulting in the nitrogen-containing CQDs as explained in XPS (Figure 3). The sp^2 domain of the carbon structure is expected to be partially distorted by the nitrogen to create sp^3 clusters, which are likely to be considered as the luminescence centers in the CQDs. We obtained some preliminary insights about the precursors that could be involved in the formation of CQDs by analyzing the samples at different preparation stages using NMR and Raman spectroscopy (as shown in Figures S14–S16). While these results insinuate that the precursors involved in the CQD formation comprise $-CH_3$ groups, a more detailed investigation in the future would be required to understand the precise mechanism.

4. CONCLUSIONS

Sonication within organic solvents is inherent to several research themes, yet the fact that this itself can lead to the formation of quantum dots has remained unexplored. In this study, we have attempted to demonstrate through acetonitrile that an organic solvent can itself serve as a source of carbon and transform into fluorescent CQDs under the effect of ultrasonication. The as-prepared CQDs are found to exhibit amphiphilicity and excitation-dependent photoluminescence. The above findings present a traditionally unknown perspective on how ultrasonication can affect the organic solvents. We have also shown that other organic solvents, such as ethylene glycol, butyronitrile, NMP, and DMSO also yield a fluorescent dispersed phase upon ultrasonication. Sonication within organic solvents is widely used in nanoscaling bulk materials to yield nanosheets as well as quantum dots, which often exhibit fluorescence (e.g., titanium disulfide,³⁷ black phosphorus^{38,39} molybdenum disulfide,⁴⁰ tungsten disulfide,⁴¹ and carbon⁴²). Our results suggest that this fluorescence could be influenced by CQDs, which are formed as a natural result of the liquid medium being exposed to ultrasonication. Moreover, the simplicity with which CQDs are obtained in this procedure presents great potential for their inexpensive, scalable production. The ability to form nitrogen-containing CQDs by using acetonitrile also sets a platform to explore the fate of ultrasonating solvents containing different heteroatoms (e.g., sulfur, phosphorus, boron, or oxygen). It would also be promising to investigate the ultrasonication of cosolvents and realize codoped QDs. Furthermore, it would be interesting to obtain more fundamental insights into this phenomenon using computational studies. This study may also open up the avenues for synthesizing pure graphene quantum dots by selecting a suitable solvent for the ultrasonication, which contains only carbon and hydrogen as its constituents. We believe that this study presents a new insight to the scientific community that would significantly contribute toward a careful design of experiments involving ultrasonication within organic solvents.

■ ASSOCIATED CONTENT

Supporting Information

The Supporting Information is available free of charge on the ACS Publications website at DOI: [10.1021/acs.jpcc.9b03975](https://doi.org/10.1021/acs.jpcc.9b03975).

Characterization, calculations for relative content, control experiments, temperature profile during sonication, survey scan of XPS, dependence of concentration on sonication, additional TEM and HRTEM images, photograph of the sample after 6 months, and optical results of other sonicated solvents (cyclohexane, butyronitrile, and ethylene glycol) ([PDF](#))

■ AUTHOR INFORMATION

Corresponding Author

*E-mail: kabeer@iitgn.ac.in.

ORCID

Kabeer Jasuja: [0000-0002-4332-0712](#)

Notes

The authors declare no competing financial interest.

■ ACKNOWLEDGMENTS

This work is supported by seed funding from IIT Gandhinagar, Core Research Grant (EMR/2017/000730) by the Science and Engineering Research Board, Fast Track Research Grant for Young Scientists (SB/FTP/ETA-114/2013), and INSPIRE Faculty Award Research Grant (DST/INSPIRE/04/2014/001601) by the Department of Science and Technology, India. Raman and XPS studies were conducted at IIT Kanpur, India. We appreciate the help of Dr. Manish Shinde (CMET, Pune, India) for the help with TEM and HR-TEM imaging. We deeply acknowledge the help extended by Palash Jena (with lifetime analysis and NMR experiments), Komal Pandey (with XRD analysis), Mahesh Kutwal (with FTIR analysis), Tarushyam Mukherjee (with NMR experiments), Rupanjali Prasad (with Raman spectroscopy), and Chetan Singh (with AFM analysis). We are indebted to Prof. Sriram Kanvah for his support with fluorescence measurements, NMR experiments, and their analysis. We are also very thankful to Prof. Arnab Dutta for helping with the NMR results. We thank the IIT Gandhinagar Central Research Facility for providing access to various instruments during this research.

■ REFERENCES

- (1) Bang, J. H.; Suslick, K. S. Applications of Ultrasound to the Synthesis of Nanostructured Materials. *Adv. Mater.* **2010**, *22*, 1039–1059.
- (2) Hernandez, Y.; et al. High-Yield Production of Graphene by Liquid-Phase Exfoliation of Graphite. *Nat. Nanotechnol.* **2008**, *3*, 563.
- (3) Zhi, C.; Bando, Y.; Tang, C.; Kuwahara, H.; Golberg, D. Large-Scale Fabrication of Boron Nitride Nanosheets and Their Utilization in Polymeric Composites with Improved Thermal and Mechanical Properties. *Adv. Mater.* **2009**, *21*, 2889–2893.
- (4) Coleman, J. N.; et al. Two-Dimensional Nanosheets Produced by Liquid Exfoliation of Layered Materials. *Science* **2011**, *331*, 568–571.
- (5) Shen, J.; et al. Liquid Phase Exfoliation of Two-Dimensional Materials by Directly Probing and Matching Surface Tension Components. *Nano Lett.* **2015**, *15*, 5449–5454.
- (6) Wang, M.; Xu, X.; Ge, Y.; Dong, P.; Baines, R.; Ajayan, P. M.; Ye, M.; Shen, J. Surface Tension Components Ratio: An Efficient Parameter for Direct Liquid Phase Exfoliation. *ACS Appl. Mater. Interfaces* **2017**, *9*, 9168–9175.
- (7) Hanlon, D.; et al. Production of Molybdenum Trioxide Nanosheets by Liquid Exfoliation and Their Application in High-Performance Supercapacitors. *Chem. Mater.* **2014**, *26*, 1751–1763.
- (8) Das, S. K.; Bedar, A.; Kannan, A.; Jasuja, K. Aqueous Dispersions of Few-Layer-Thick Chemically Modified Magnesium Diboride

- Nanosheets by Ultrasonication Assisted Exfoliation. *Sci. Rep.* **2015**, *5*, 10522.
- (9) Das, S. K.; Jasuja, K. Chemical Exfoliation of Layered Magnesium Diboride to Yield Functionalized Nanosheets and Nanoaccordions for Potential Flame Retardant Applications. *ACS Appl. Nano Mater.* **2018**, *1*, 1612–1622.
- (10) Naguib, M.; Mashtalir, O.; Carle, J.; Presser, V.; Lu, J.; Hultman, L.; Gogotsi, Y.; Barsoum, M. W. Two-Dimensional Transition Metal Carbides. *ACS Nano* **2012**, *6*, 1322–1331.
- (11) Wu, M.; Zhan, J.; Geng, B.; He, P.; Wu, K.; Wang, L.; Xu, G.; Li, Z.; Yin, L.; Pan, D. Scalable Synthesis of Organic-Soluble Carbon Quantum Dots: Superior Optical Properties in Solvents, Solids, and Leds. *Nanoscale* **2017**, *9*, 13195–13202.
- (12) Chen, B. B.; Liu, Z. X.; Deng, W. C.; Zhan, L.; Liu, M. L.; Huang, C. Z. A Large-Scale Synthesis of Photoluminescent Carbon Quantum Dots: A Self-Exothermic Reaction Driving the Formation of the Nanocrystalline Core at Room Temperature. *Green Chem.* **2016**, *18*, 5127–5132.
- (13) Wang, L.; et al. Gram-Scale Synthesis of Single-Crystalline Graphene Quantum Dots with Superior Optical Properties. *Nat. Commun.* **2014**, *5*, 5357.
- (14) Ding, Z.; Li, F.; Wen, J.; Wang, X.; Sun, R. Gram-Scale Synthesis of Single-Crystalline Graphene Quantum Dots Derived from Lignin Biomass. *Green Chem.* **2018**, *20*, 1383–1390.
- (15) Wang, Y.; Meng, Y.; Wang, S.; Li, C.; Shi, W.; Chen, J.; Wang, J.; Huang, R. Direct Solvent-Derived Polymer-Coated Nitrogen-Doped Carbon Nanodots with High Water Solubility for Targeted Fluorescence Imaging of Glioma. *Small* **2015**, *11*, 3575–3581.
- (16) Lei, W.; Portehault, D.; Dimova, R.; Antonietti, M. Boron Carbon Nitride Nanostructures from Salt Melts: Tunable Water-Soluble Phosphors. *J. Am. Chem. Soc.* **2011**, *133*, 7121–7127.
- (17) Zhang, Y.-Q.; Ma, D.-K.; Zhuang, Y.; Zhang, X.; Chen, W.; Hong, L.-L.; Yan, Q.-X.; Yu, K.; Huang, S.-M. One-Pot Synthesis of N-Doped Carbon Dots with Tunable Luminescence Properties. *J. Mater. Chem.* **2012**, *22*, 16714–16718.
- (18) Tang, L.; Ji, R.; Li, X.; Teng, K. S.; Lau, S. P. Energy-Level Structure of Nitrogen-Doped Graphene Quantum Dots. *J. Mater. Chem. C* **2013**, *1*, 4908–4915.
- (19) Wu, J.; et al. A Metal-Free Electrocatalyst for Carbon Dioxide Reduction to Multi-Carbon Hydrocarbons and Oxygenates. *Nat. Commun.* **2016**, *7*, 13869.
- (20) Zheng, X. T.; Ananthanarayanan, A.; Luo, K. Q.; Chen, P. Glowing Graphene Quantum Dots and Carbon Dots: Properties, Syntheses, and Biological Applications. *Small* **2015**, *11*, 1620–1636.
- (21) Ding, H.; Wei, J.-S.; Xiong, H.-M. Nitrogen and Sulfur Co-Doped Carbon Dots with Strong Blue Luminescence. *Nanoscale* **2014**, *6*, 13817–13823.
- (22) Tan, J.; Zou, R.; Zhang, J.; Li, W.; Zhang, L.; Yue, D. Large-Scale Synthesis of N-Doped Carbon Quantum Dots and Their Phosphorescence Properties in a Polyurethane Matrix. *Nanoscale* **2016**, *8*, 4742–4747.
- (23) Li, Y.; Zhao, Y.; Cheng, H.; Hu, Y.; Shi, G.; Dai, L.; Qu, L. Nitrogen-Doped Graphene Quantum Dots with Oxygen-Rich Functional Groups. *J. Am. Chem. Soc.* **2012**, *134*, 15–18.
- (24) Teng, X.; Ma, C.; Ge, C.; Yan, M.; Yang, J.; Zhang, Y.; Morais, P. C.; Bi, H. Green Synthesis of Nitrogen-Doped Carbon Dots from Konjac Flour with "Off-on" Fluorescence by Fe³⁺ and L-Lysine for Bioimaging. *J. Mater. Chem. B* **2014**, *2*, 4631–4639.
- (25) Holá, K.; Sudolská, M.; Kalytchuk, S.; Nachtigalová, D.; Rogach, A. L.; Otyepka, M.; Zboril, R. Graphitic Nitrogen Triggers Red Fluorescence in Carbon Dots. *ACS Nano* **2017**, *11*, 12402–12410.
- (26) Park, Y. R.; Jeong, H. Y.; Seo, Y. S.; Choi, W. K.; Hong, Y. J. Quantum-Dot Light-Emitting Diodes with Nitrogen-Doped Carbon Nanodot Hole Transport and Electronic Energy Transfer Layer. *Sci. Rep.* **2017**, *7*, 46422.
- (27) Zhang, J.; Shen, W.; Pan, D.; Zhang, Z.; Fang, Y.; Wu, M. Controlled Synthesis of Green and Blue Luminescent Carbon Nanoparticles with High Yields by the Carbonization of Sucrose. *New J. Chem.* **2010**, *34*, 591–593.
- (28) Yuan, H.; Yu, J.; Feng, S.; Gong, Y. Highly Photoluminescent Ph-Independent Nitrogen-Doped Carbon Dots for Sensitive and Selective Sensing of P-Nitrophenol. *RSC Adv.* **2016**, *6*, 15192–15200.
- (29) Peng, J.; et al. Graphene Quantum Dots Derived from Carbon Fibers. *Nano Lett.* **2012**, *12*, 844–849.
- (30) Qu, D.; Zheng, M.; Li, J.; Xie, Z.; Sun, Z. Tailoring Color Emissions from N-Doped Graphene Quantum Dots for Bioimaging Applications. *Light: Sci. Appl.* **2015**, *4*, No. e364.
- (31) Pan, D.; Zhang, J.; Li, Z.; Wu, M. Hydrothermal Route for Cutting Graphene Sheets into Blue-Luminescent Graphene Quantum Dots. *Adv. Mater.* **2010**, *22*, 734–738.
- (32) Suryawanshi, A.; Biswal, M.; Mhamane, D.; Gokhale, R.; Patil, S.; Guin, D.; Ogale, S. Large Scale Synthesis of Graphene Quantum Dots (Gqds) from Waste Biomass and Their Use as an Efficient and Selective Photoluminescence on-Off-on Probe for Ag⁺ Ions. *Nanoscale* **2014**, *6*, 11664–11670.
- (33) Chen, X.; Jin, Q.; Wu, L.; Tung, C.; Tang, X. Synthesis and Unique Photoluminescence Properties of Nitrogen-Rich Quantum Dots and Their Applications. *Angew. Chem., Int. Ed.* **2014**, *53*, 12542–12547.
- (34) Kumar, V. B.; Porat, Z.; Gedanken, A. Facile One-Step Sonochemical Synthesis of Ultrafine and Stable Fluorescent C-Dots. *Ultrason. Sonochem.* **2016**, *28*, 367–375.
- (35) Kumar, V. B.; Borenstein, A.; Markovsky, B.; Aurbach, D.; Gedanken, A.; Talianker, M.; Porat, Z. Activated Carbon Modified with Carbon Nanodots as Novel Electrode Material for Supercapacitors. *J. Phys. Chem. C* **2016**, *120*, 13406–13413.
- (36) Wei, K.; Li, J.; Ge, Z.; You, Y.; Xu, H. Sonochemical Synthesis of Highly Photoluminescent Carbon Nanodots. *RSC Adv.* **2014**, *4*, 52230–52234.
- (37) Liu, Y.; et al. Atomic Layered Titanium Sulfide Quantum Dots as Electrocatalysts for Enhanced Hydrogen Evolution Reaction. *Adv. Mater. Interfaces* **2018**, *5*, 1700895.
- (38) Fu, N.; et al. Black Phosphorus Quantum Dots as Dual-Functional Electron-Selective Materials for Efficient Plastic Perovskite Solar Cells. *J. Mater. Chem. A* **2018**, *6*, 8886–8894.
- (39) Sun, Z.; Xie, H.; Tang, S.; Yu, X.-F.; Guo, Z.; Shao, J.; Zhang, H.; Huang, H.; Wang, H.; Chu, P. K. Ultrasmall Black Phosphorus Quantum Dots: Synthesis and Use as Photothermal Agents. *Angew. Chem., Int. Ed.* **2015**, *54*, 11526–11530.
- (40) Gopalakrishnan, D.; Damien, D.; Shajumon, M. M. MoS₂ Quantum Dot-Interspersed Exfoliated MoS₂ Nanosheets. *ACS Nano* **2014**, *8*, 5297–5303.
- (41) Zhou, L.; Yan, S.; Wu, H.; Song, H.; Shi, Y. Facile Sonication Synthesis of Ws₂ Quantum Dots for Photoelectrochemical Performance. *Catalysts* **2017**, *7*, 18.
- (42) Prasad, K. P.; Chen, Y.; Sk, M. A.; Than, A.; Wang, Y.; Sun, H.; Lim, K.-H.; Dong, X.; Chen, P. Fluorescent Quantum Dots Derived from Pedot and Their Applications in Optical Imaging and Sensing. *Mater. Horiz.* **2014**, *1*, 529–534.
- (43) Xu, S.; Li, D.; Wu, P. One-Pot, Facile, and Versatile Synthesis of Monolayer MoS₂/WS₂ Quantum Dots as Bioimaging Probes and Efficient Electrocatalysts for Hydrogen Evolution Reaction. *Adv. Funct. Mater.* **2015**, *25*, 1127–1136.
- (44) Kozák, O.; Datta, K. K. R.; Greplová, M.; Ranc, V.; Kašík, J.; Zbořil, R. Surfactant-Derived Amphiphilic Carbon Dots with Tunable Photoluminescence. *J. Phys. Chem. C* **2013**, *117*, 24991–24996.
- (45) Liu, M. L.; Chen, B. B.; Li, C. M.; Huang, C. Z. Carbon Dots: Synthesis, Formation Mechanism, Fluorescence Origin and Sensing Applications. *Green Chem.* **2019**, *21*, 449–471.
- (46) Song, Z.; Quan, F.; Xu, Y.; Liu, M.; Cui, L.; Liu, J. Multifunctional N,S Co-Doped Carbon Quantum Dots with Ph- and Thermo-Dependent Switchable Fluorescent Properties and Highly Selective Detection of Glutathione. *Carbon* **2016**, *104*, 169–178.
- (47) Xu, Y.; Jia, X.-H.; Yin, X.-B.; He, X.-W.; Zhang, Y.-K. Carbon Quantum Dot Stabilized Gadolinium Nanoprobe Prepared Via a One-

Pot Hydrothermal Approach for Magnetic Resonance and Fluorescence Dual-Modality Bioimaging. *Anal. Chem.* **2014**, *86*, 12122–12129.

(48) He, G.; Shu, M.; Yang, Z.; Ma, Y.; Huang, D.; Xu, S.; Wang, Y.; Hu, N.; Zhang, Y.; Xu, L. Microwave Formation and Photoluminescence Mechanisms of Multi-States Nitrogen Doped Carbon Dots. *Appl. Surf. Sci.* **2017**, *422*, 257–265.

(49) Tao, H.; Zhang, Y.; Gao, Y.; Sun, Z.; Yan, C.; Texter, J. Scalable Exfoliation and Dispersion of Two-Dimensional Materials - an Update. *Phys. Chem. Chem. Phys.* **2017**, *19*, 921–960.

(50) Suslick, K. S.; Hammerton, D. A.; Cline, R. E. Sonochemical Hot Spot. *J. Am. Chem. Soc.* **1986**, *108*, 5641–5642.

(51) Sun, X.; Li, Y. Colloidal Carbon Spheres and Their Core/Shell Structures with Noble-Metal Nanoparticles. *Angew. Chem., Int. Ed.* **2004**, *43*, 597–601.

(52) Dong, Y.; Shao, J.; Chen, C.; Li, H.; Wang, R.; Chi, Y.; Lin, X.; Chen, G. Blue Luminescent Graphene Quantum Dots and Graphene Oxide Prepared by Tuning the Carbonization Degree of Citric Acid. *Carbon* **2012**, *50*, 4738–4743.

(53) Li, H.; He, X.; Liu, Y.; Huang, H.; Lian, S.; Lee, S.-T.; Kang, Z. One-Step Ultrasonic Synthesis of Water-Soluble Carbon Nanoparticles with Excellent Photoluminescent Properties. *Carbon* **2011**, *49*, 605–609.

(54) Tang, L.; et al. Deep Ultraviolet Photoluminescence of Water-Soluble Self-Passivated Graphene Quantum Dots. *ACS Nano* **2012**, *6*, 5102–5110.